Structural Stability and Dynamics of Hydrogenated and Perdeuterated Cytochrome P450cam (CYP101)†

Flora Meilleur,‡ Jörg Contzen,§ Dean A. A. Myles,‡ and Christiane Jung*,§

EMBL−Grenoble Outstation, BP 181, 38042 Grenoble Cedex 9, France, and Max-Delbrück Center for Molecular Medicine, 13125 Berlin, Germany

Received March 25, 2004; Revised Manuscript Received May 12, 2004

ABSTRACT: Perdeuterated and hydrogenated cytochrome P450cam (P450cam), from *Pseudomonas putida*, has been characterized concerning thermal stability and structural dynamics. For the first time, Fourier transform infrared (FTIR) spectroscopy was used to characterize a perdeuterated protein. The secondary structure compositions were determined from the fitted amide I′ spectral region, giving band populations at 10 °C for the perdeuterated protein of 22% between 1605 and 1624 cm^{-1} (β-sheets), 47% between 1633 and 1650 cm^{-1} (α-helix (29%) plus unordered/3_{10}-helix (18%)), and 28% between 1657 and 1677 cm^{-1} (turns) and for the hydrogenated protein of 22% between 1610 and 1635 cm^{-1} (β-sheets), 52% between 1640 and 1658 cm^{-1} (α-helix (41%) plus unordered/3_{10}-helix (11%)), and 24% between 1665 and 1680 cm^{-1} (turns).Thermal unfolding experiments revealed that perdeuterated P450cam was less stable than the hydrogenated protein. The midpoint transition temperatures were 60.8 and 64.4 °C for the perdeuterated and hydrogenated P450cam, respectively. Step-scan time-resolved FTIR was applied to the P450cam−CO complex to study the ligand-rebinding process after flash photolysis. Rebinding of the ligand occurred with the same kinetics and rate constants k_{on}, 8.9×10^4 and 8.3×10^4 M^{-1} s^{-1} for the perdeuterated and hydrogenated P450cam, respectively.Perdeuterated P450cam was expressed for a neutron crystallographic study to determine the specific hydration states and hydrogen-bonding networks at the active site. The analyses presented here show that perdeuterated P450cam is structurally similar to its hydrogenated counterpart, despite its reduced thermal stability, suggesting that information obtained from the neutron structure will be representative of the normal hydrogenated P450cam.

Cytochrome P450s (P450s) are a superfamily of heme-containing enzymes found throughout the biosphere. P450s are involved in a broad range of biochemical processes including drug metabolism, xenobiotics degradation, or steroid biosynthesis. They mainly catalyze hydroxylation reactions (*1*). Cytochrome P450cam from *Pseudomonas putida* (P450cam)[1] is the best-characterized member of the P450 family. It catalyzes the regio- and stereospecific hydroxylation of its physiological substrate (1*R*)-camphor to 5-*exo*-hydroxycamphor by incorporating one oxygen atom from molecular oxygen. The other oxygen atom is reduced to water. Proton transfer is critical for the cleavage of the O−O bond of the heme-bound O_2. Identification of the proton delivery pathway at the active site of cytochrome P450cam could contribute to the understanding of cytochrome P450's oxygen activation mechanism. Recent analyses of several intermediates of the reaction pathway of cytochrome P450cam obtained by X-ray crystallography have suggested a key role for an internal water network composed of five water molecules and the highly conserved residues Asp251 and Thr252 (*2*). Interaction between these residues and specifically bound water molecules through complex hydrogen bond networks may provide the needed protons for the reaction. Unfortunately, hydrogen atom positions cannot be determined at the resolution given for these analyses because hydrogen atoms are very weak X-ray scatterers. They are therefore difficult to localize in proteins and water molecules using X-ray crystallography alone unless ultra-high-resolution data are available. In contrast, the scattering powers of hydrogen or deuterium (^{2}H or D) for neutrons are similar to those of the other atoms found in a protein (C, N, O, S). Neutron crystallography thus allows direct localization of hydrogen/deuterium at resolutions of 1.5−2.0 Å (*3*−*10*). We aim to determine the neutron structure of P450cam to further characterize the active site hydrogen bond networks. In particular, the neutron structure would help to determine the orientation of waters W901 and W902 in oxy-P450cam (*2*), with the result that the interactions among amino acid residues, water molecules, and the O_2-bound molecule could be unambiguously determined. However, to reduce the background scattering arising from the large incoherent cross section of hydrogen and to enhance

† This study was supported by Deutsche Forschungsgemeinschaft Grants SK35/3-5 and Ju229/4-3 (to C.J.).

* To whom correspondence should be addressed. Phone: +49-30-94063370. Fax: +49-30-94062548. E-mail: cjung@mdc-berlin.de.

‡ EMBL−Grenoble Outstation.

§ Max-Delbrück Center for Molecular Medicine.

[1] Abbreviations: FTIR, Fourier transform infrared spectroscopy; P450cam, cytochrome P450cam from *Pseudomonas putida*, CYP101; P450cam-bound, P450cam bound with (1*R*)-camphor; P450cam-(C334A), mutant of P450cam where cysteine at position 334 was replaced by alanine; OD, optical density; HCDC, high-cell-density cultivations; TEV, tobacco etch virus; EDTA, ethylenediaminetetraacetic acid; DTT, dithiothreitol; ESI-MS, electrospray ionization mass spectrometry; IPTG, isopropyl β-D-thiogalactopyranoside.

10.1021/bi049418q CCC: $27.50
Published on Web 06/18/2004

the visibility of hydrogen positions, perdeuterated protein—both exchangeable and nonexchangeable (which means covalently bound) hydrogens are replaced with deuterium—are preferred to collect neutron crystallography data (*6*). To be sure that the neutron structure of perdeuterated P450cam will be a true representation of the native hydrogenated protein, we have intended to characterize structurally and physicochemically the perdeuterated P450cam. We have recently demonstrated that the structure of perdeuterated cytochrome P450cam determined by X-ray crystallography is not significantly affected by perdeuteration (unpublished experiments). However, the physicochemical properties such as structural stability and dynamics might be different between perdeuterated and hydrogenated proteins (*11*). In this study we apply Fourier transform infrared spectroscopy (FTIR) to investigate the thermal stability and protein unfolding behavior using the amide bands as spectroscopic probes. The structural dynamics is studied with step-scan time-resolved FTIR by monitoring the rebinding kinetics of the photodissociated CO ligand at the ligand stretch vibration band and at the amide spectral signals. Thus, FTIR spectroscopy allows global structural changes as well as local effects to be characterized when using the appropriate spectroscopic probes. It will be shown that there is no difference in the CO-rebinding kinetics. In contrast, the perdeuterated P450cam turned out to be less thermally stable than the hydrogenated one.

MATERIALS AND METHODS

Cloning, Expression, and Purification of Perdeuterated Cytochrome P450cam-(C334A) Mutant. The gene encoding wild-type P450cam was amplified by polymerase chain reaction (PCR) using the pUS200 vector (*12*) as a template and inserted into the *Nco*I/*Not*I-digested expression vector pET-M11 (EMBL) that contained a coding sequence for N-terminal His_6-tag and a recognition site for TEV protease. The forward and reverse oligonucleotide primers used were 5′-CTC CCA TGT TAT TAT ACC GCT TTG G-3′ and 5′-CCA GGA GAA GGT CTC CCA TGA CGA CTG-3′, respectively. The QuickChange XL site-directed mutagenesis kit (Stratagene) was used to insert the C334A point mutation. The forward oligonucleotide primer designed was 5′-CGC GAA AAC GCC GCC CCG ATG CAC GTC GAC TTC AGT CGC-3′. This mutation avoids the dimerization of the protein via the intermolecular S−S bridge between the cysteines at the 334-postion in the wild-type protein (*13*, *14*). The single C334A point mutation was verified by DNA sequencing. The plasmid was transformed into *Escherichia coli* strain BL21 (DE3) (Novagen Inc.).

High-cell-density cultivations (HCDCs) were performed to maximize the protein production. Cells were cultured in minimal medium [6.86 g/L $(NH_4)_2SO_4$, 1.56 g/L KH_2PO_4, 6.48 g/L $Na_2HPO_4 \cdot 2H_2O$, 0.49 g/L $(NH_4)_2$-H-citrate, 0.25 g/L $MgSO_4 \cdot 7H_2O$, 1.0 mL/L (0.5 g/L $CaCl_2 \cdot 2H_2O$, 16.7 g/L $FeCl_3 \cdot 6H_2O$, 0.18 g/L $ZnSO_4 \cdot 7H_2O$, 0.16 g/L $CuSO_4 \cdot 5H_2O$, 0.15 g/L $MnSO_4 \cdot 4H_2O$, 0.18 g/L $CoCl_2 \cdot 6H_2O$, 20.1 g/L EDTA), 5 g/L glycerol, 40 mg/L kanamycin] in 2 L bioreactors (Infors). For preparation of fully deuterated medium, hydrated mineral salts were dried out and labile hydrogens were exchanged for deuterium by dissolution in a minimal volume of D_2O and freeze-drying. Perdeuterated d_8-glycerol (CIL) was used as carbon source. Cells were adapted to fully deuterated medium in three steps. Freshly transformed cells were plated on Luria Bertani solid medium. A colony was selected and plated on solid hydrogenated minimal medium. After overnight growth, cells were plated on fully deuterated solid minimal medium. Liquid deuterated minimal medium was then inoculated with the adapted cells. HCDCs were achieved in two phases: once the initially provided glycerol was consumed (batch phase), cells were fed continuously with fresh feeding solution [8% d_8-glycerol (30% h_8-glycerol for hydrogenated culture), 0.2% $MgSO_4$, and 40 mg/L kanamycin] (fed-batch phase). When the optical density (OD) at 600 nm of perdeuterated culture reached 5.0 (7.0 for hydrogenated culture), the medium was supplemented with hydrogenated camphor and hydrogenated δ-aminolevulinic acid (heme precursor) dissolved in minimal medium to final concentrations of 1 mM. Protein overexpression was induced when the OD reached 7.0 (12.0 for hydrogenated culture) with hydrogenated IPTG to a final concentration of 0.5 mM. The temperature was set at 30 °C and the dissolved oxygen to 30% during the whole culture. The cells were harvested 24 h after induction and stored at −80 °C until further use.

Purifications of hydrogenated and perdeuterated P450cam-(C334A) were made in hydrogenated buffers using the same protocols. All procedures were made at 0−4 °C, unless specified. A 10−15 g sample of frozen cells was resuspended in 50 mL of lysis buffer [buffer A: 50 mM potassium phosphate, pH 7.6, 250 mM KCl, 1 mM (1*R*)-camphor, 5 mM β-mercaptoethanol, one protease EDTA-free tablet (Roche)/50 mL] and lysed by sonication on an ice/dry ice/ethanol mixture. Cell debris and DNA were removed by centrifugation at 15000*g* force for 30 min. The supernatant was loaded onto a cobalt affinity column (Clontech), previously equilibrated against buffer A. Contaminants were removed by washing the column with 20 column volumes of buffer A containing 5 mM imidazole. The protein was eluted with 3 column volumes of buffer A containing 90 mM imidazole. The fractions containing P450cam-(C334A) were pooled and concentrated to a volume of 2.5 mL (Centriprep YM 10). Buffer A was exchanged to His_6-tag cleavage buffer (50 mM potassium phosphate buffer, pH 7.6, 250 mM KCl, 1 mM (1*R*)-camphor, 0.5 mM EDTA, 1 mM DTT) using a desalting column (Amersham Pharmacia). TEV protease was added in a molar ratio of 1:100. Cleavage was complete after 15 h at 15 °C. The buffer was then exchanged to 50 mM potassium phosphate buffer, pH 7.0, 1 mM (1R)-camphor and the sample rerun over the cobalt column to remove the cleaved His_6-tag and the TEV, which is itself His_6-tagged. The purity of the protein was assessed by measuring an absorbance ratio (392 nm/280 nm) of 1.4. The level of deuterium incorporation was determined by mass spectrometry. ESI-MS spectra were recorded for both proteins, giving experimental molecular masses of 46.764 and 49.272 kDa for the hydrogenated and perdeuterated P450cam-(C334A), respectively, purified in hydrogenated buffers. Hydrogenated P450cam-(C334A) and perdeuterated P450cam-(C334A) purified in hydrogenated buffers have theoretical molecular masses of 46.762 and 46.762 + [2.534 (nonexchangeable deuterium) × 1.006 (the mass difference between deuterium and hydrogen)] = 49.311 kDa, respectively. The level of deuteration was therefore estimated to be (49.272 − 46.764)/(49.311 − 46.762) = 98%. For IR

measurements both hydrogenated P450cam-(C334A) and perdeuterated P450cam-(C334A) were dialyzed against deuterated phosphate buffer (100 mM potassium phosphate buffer, pD 7.4 corresponding to an original protonic pH 7.0 (*15*), 1 mM (1*R*)-camphor) by six exchanges of the buffer (5 mL) for a volume of the protein solution of 100 μL within 72 h.

FTIR Thermal Unfolding Studies. Infrared spectra were recorded using the Bruker IFS66 FTIR spectrometer equipped with a liquid-nitrogen-cooled broad-band MCT detector (Bruker D316). The protein solution at room temperature was placed in a demountable thermostated cell with CaF_2 windows separated by a 23 μm thick Teflon spacer. The temperature was regulated using the Haake F8 cryothermostat with an accuracy of $\pm$0.1 °C. The spectral resolution was set to 2 cm^{-1} in a double-sided/forward−backward acquisition mode. Fourier transformations of 100−1000 co-added interferograms of both sample and background were performed with the Blackman−Harris three-term apodization function and a zero-filling factor of 4 in the region of 800−4500 cm^{-1}. The phase correction was made according to Mertz using a phase resolution of 128 cm^{-1}.

Residual water vapor absorption was interactively subtracted from the sample spectra. The background spectrum was taken with the buffer used in the last dialysis step for the H_2O/D_2O exchange of the proteins.

Absorption spectra were obtained from the negative decadic logarithm of the ratio of the sample single-channel spectrum to the single-channel spectrum of the buffer background. The spectra were scaled to the same peak amplitude of the amide I′ band. The absorption spectra were baseline corrected with the rubber band method using the baseline points at 1500 and 1800 cm^{-1}, smoothed with 21 points using the Savitzky−Golay algorithm, and deconvoluted between 1800 and 1495 cm^{-1} using the deconvolution factor of 5000 and the noise reduction factor of 0.25 using the OPUS 3.0 Bruker software. The deconvoluted spectra in the range between 1595 and 1700 cm^{-1} were fitted with Voigt functions using a nonlinear least-squares curve-fitting program (*16*). The initial number of bands and the fit start values for the band positions were chosen from the minima in the second-derivative spectrum of the original absolute spectra. It turned out that the best fit was obtained with 10 Voigt functions as previously observed (*17*). The spectra at the different temperatures were area-normalized. The relative areas of the single bands were used to determine the fraction of the secondary structure elements. The amide I′ band spectra were not corrected by the overlapping absorption bands of the amino acid side chains as described in our previous work (*17*) because the absorption spectra of free perdeuterated amino acids needed for the correction are not available.

Unfolding curves for the amide I′ were constructed from the plot of the absorbance difference ΔA between the maximum and the minimum in the difference spectra, obtained from the area-normalized deconvoluted spectra at temperature T minus the spectrum at 10 °C (ΔA(1616.04−1657.50 cm^{-1}) for hydrogenated P450cam and ΔA(1609.29−1640.63 cm^{-1}) for perdeuterated P450cam), versus the temperature. In addition, unfolding curves were determined from the fraction of the β-sheets and α-helices as a function of the temperature.

Unfolding curves for the amide II band (bending of N−H mixed with C−N stretching in the protein core (*16*)) were obtained from the increasing amplitude of the negative band at about 1550 cm^{-1} in the temperature difference spectra (not deconvoluted) with increasing temperature.

All unfolding curves were fitted with eq 1, which corresponds to a sigmoid curve overlaid with a linear temperature dependence of the absorbance of the folded ($a + bT$) and unfolded ($c + dT$) states (*18*). T, $T_{1/2}$, and ΔH are the temperature, the half-transition temperature, and the enthalpy of unfolding, respectively. The entropy ΔS for the unfolding can be calculated from $\Delta H/T_{1/2}$.

$$A = \frac{(a + bT) + (c + dT)\exp\left[-\frac{\Delta H}{R}\left(\frac{1}{T} - \frac{1}{T_{1/2}}\right)\right]}{\left(1 + \exp\left[-\frac{\Delta H}{R}\left(\frac{1}{T} - \frac{1}{T_{1/2}}\right)\right]\right)} \quad (1)$$

FTIR CO Flash Photolysis Study. P450cam protein in deuterated 100 mM potassium phosphate buffer, pD 7.4 corresponding to an original protonic pH 7.0 (*15*), 1 mM (1*R*)-camphor has been concentrated to 1 mM protein concentration using Microcon-30 (Millipore) ultrafiltration devices. Equal volumes of protein stock solution and glycerol-d_3 (Aldrich) were mixed, (1*R*)-camphor was added from ethanolic stock solution (0.7 M) to keep the protein in the substrate-bound state, and the resulting mixture was reduced by addition of a nitrogen-purged sodium dithionite solution (1 M). The final sample composition contained 50 mM potassium phosphate buffer, pD 7.4, 50% (v/v) glycerol-d_3, 30 mM (1*R*)-camphor, and 130 mM sodium dithionite. Carbon monoxide was passed over the sample surface for 3 min immediately before the sample was loaded into CaF_2 sample cuvettes with a 23.4 μm Teflon spacer. The P450−CO concentration was checked by reading the absorbance of the Soret band at 446 nm (ϵ = 121 mM^{-1} cm^{-1}) directly observed in the IR cell.

Time-resolved infrared spectra were recorded on a Bruker IFS66 FTIR spectrometer with the step-scan option. The experimental setup and the processing of the interferograms have been described in detail elsewhere (*19*). Samples were photolyzed by the 532 nm radiation of a frequency-doubled Nd:YAG laser (Surelite-I, Continuum, Santa Clara, CA) with a 2.3 mJ pulse energy. For each experiment, 1332 interferogram points were measured to get 4 cm^{-1} spectral resolution. At each interferogram position, the time courses of 48 sample excitations were averaged to get a sufficient signal-to-noise ratio. The experiment was repeated three times with each sample, and the results were averaged to further improve the signal-to-noise ratio. The integrity of each sample was checked before and after the experiments by UV−vis spectroscopy without any remarkable decay in the P450−CO concentration or formation of the inactive P420 form.

Absorbance difference spectra were calculated from the single-channel intensity spectra $I(t)$ and the dark-intensity spectrum I_D as $\Delta\text{Abs} = -[\log[I(t)/I_D]]$. The experimental time course was fitted to a second-order reaction kinetic model, assuming a simple one-state model [P450 + CO → P450−CO] for the carbon monoxide rebinding at 300 K, but neglecting thermal dissociation processes (*19*):

$$\Delta\mathrm{Abs} = \epsilon l\left([\mathrm{P450}]_0\frac{\exp[k_{on}t([\mathrm{CO}]_0-[\mathrm{P450}]_0)]-1}{\exp[k_{on}t([\mathrm{CO}]_0-[\mathrm{P450}]_0)]-\frac{[\mathrm{P450}]_0}{[\mathrm{CO}]_0}}-[\mathrm{P450CO}]_\infty\right) \quad (2)$$

ϵ is the molar extinction coefficient, and l represents the sample path length. $[P450]_0$ and $[CO]_0$ are the initial P450cam and carbon monoxide concentrations, respectively, generated by the laser flash, and $[P450CO]_\infty$ is the carbon monoxide complex concentration in the dark sample. The second-order rebinding constant k_{on} and ϵl have been determined by the nonlinear least-squares fitting procedure.

RESULTS

Secondary Structure Analysis and Thermal Unfolding. Figure 1 shows the absolute absorption spectra of the hydrogenated and perdeuterated P450cam-(C334A) mutant in the spectral range between 1800 and 1360 cm^{-1}. The spectrum for the hydrogenated protein exhibits the maximum of the amide I′ band at 1651.7 cm^{-1} and the tyrosine ring vibration band at 1516.2 cm^{-1} (1515.3 cm^{-1} in the second-derivative spectrum). The broad amide II bands for the N−H and the N−D bending are centered at about 1550 and 1448 cm^{-1}, respectively. In addition, there is a weak band at 1720.2 cm^{-1} (1722.1 cm^{-1} in the second-derivative spectrum) assigned previously to the CO stretch band of the COOD group of the propionic acid substituents of the porphyrin ring involved in salt bridges to either His355 (*20*) or Arg299 and Asp297 (*19*), respectively. In the perdeuterated protein, the amide I′ band is shifted by ∼10 cm^{-1} to lower wavenumbers (1641.6 cm^{-1}) while the amide II band (N−H bending) is shifted to higher wavenumbers by ∼10 cm^{-1} (∼1558.6 cm^{-1}). The amide II′ band (N−D bending) in the absolute spectra is almost at the same position in both proteins. However, the second-derivative spectra show two minima in this region which are shifted by ∼4 cm^{-1} to higher wavenumbers in the perdeuterated protein. The band at 1720.2 cm^{-1} is not changed, and the tyrosine peak is missing. Only in the second-derivative spectrum a very small peak at ∼1515 cm^{-1} is visible which may result from the tyrosine vibration of a small fraction of the protein molecules which are not perdeuterated. The maxima and shoulders in the deconvoluted amide I′ spectra in Figure 2 correspond to the minima in the second-derivative spectrum shown in Figure 1. The difference spectra from the spectrum at 10 °C (insets in Figure 2) show between 10 and 50 °C another pattern in addition to the changes between 50 and 80 °C, indicating qualitatively different conformational changes in both these temperature ranges. Unfolding curves obtained from the plot of the absorbance difference between the maxima (β-sheet region) and minima (α-helix region) in the difference spectra (Figure 3A) show that the perdeuterated protein is less stable ($T_{1/2}$(D) ≈ 60 °C) compared to the hydrogenated protein ($T_{1/2}$(H) ≈ 64 °C). The thermodynamic parameters are ΔH(D) = 73 ± 12 kcal/mol and ΔS(D) = 219 ± 36 cal/(K·mol) and ΔH(H) = 80 ± 5 kcal/mol and ΔS(H) = 236 ± 16 cal/(K·mol) for the perdeuterated and hydrogenated protein, respectively.

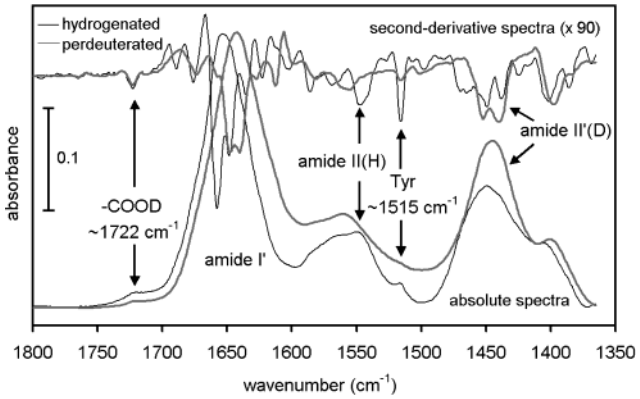

FIGURE 1: FT infrared absorption spectra and their second-derivative spectra of the hydrogenated (solid black line) and perdeuterated (solid gray line) P450cam-(C334A) mutant. Only for this figure the left-to-right direction for higher-to-lower wavenumbers is shown as commonly used in infrared spectroscopy.

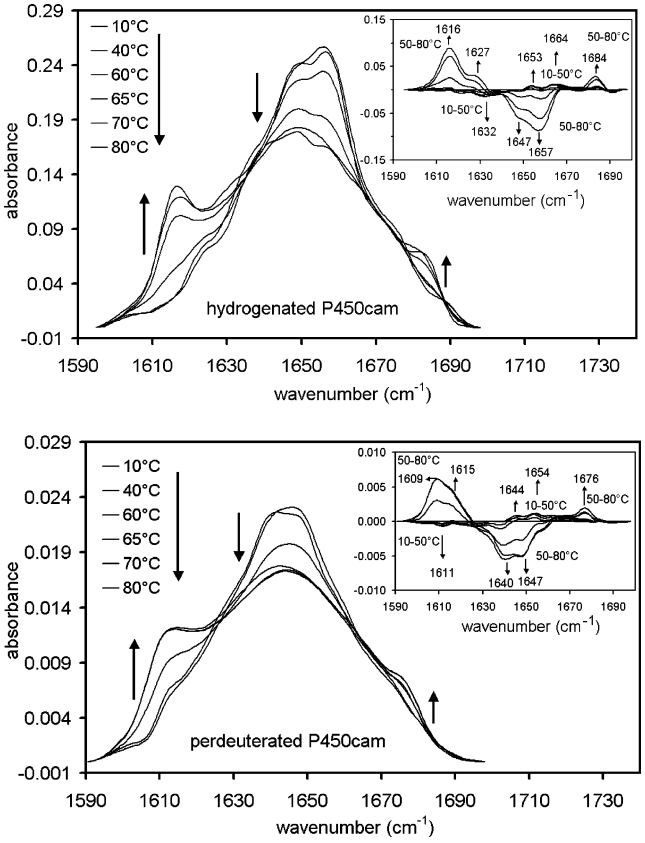

FIGURE 2: Deconvoluted infrared spectra in the amide I′ region for (A, top) the hydrogenated P450cam-(C334A) mutant and (B, bottom) the perdeuterated P450cam-(C334A) mutant at selected temperatures. All spectra are normalized to the same area. The insets show the difference spectra from the spectrum at 10 °C.

The deconvoluted spectra were fitted with 10 Voigt functions which gave a stable and very good fit with physically reasonable band positions and bandwidths (Figure 4A,B). Although each of the 10 bands shows similar positions in the hydrogenated and perdeuterated proteins, they have to be assigned to different secondary structure elements to consider the shift of ∼10 cm^{-1} due to the perdeuteration (Tables 1 and 2). The correctness of this assignment can easily be justified when the whole deconvoluted spectrum for the perdeuterated protein is back-shifted by ∼10 cm^{-1}, leading to an overlay with the spectrum of the hydrogenated

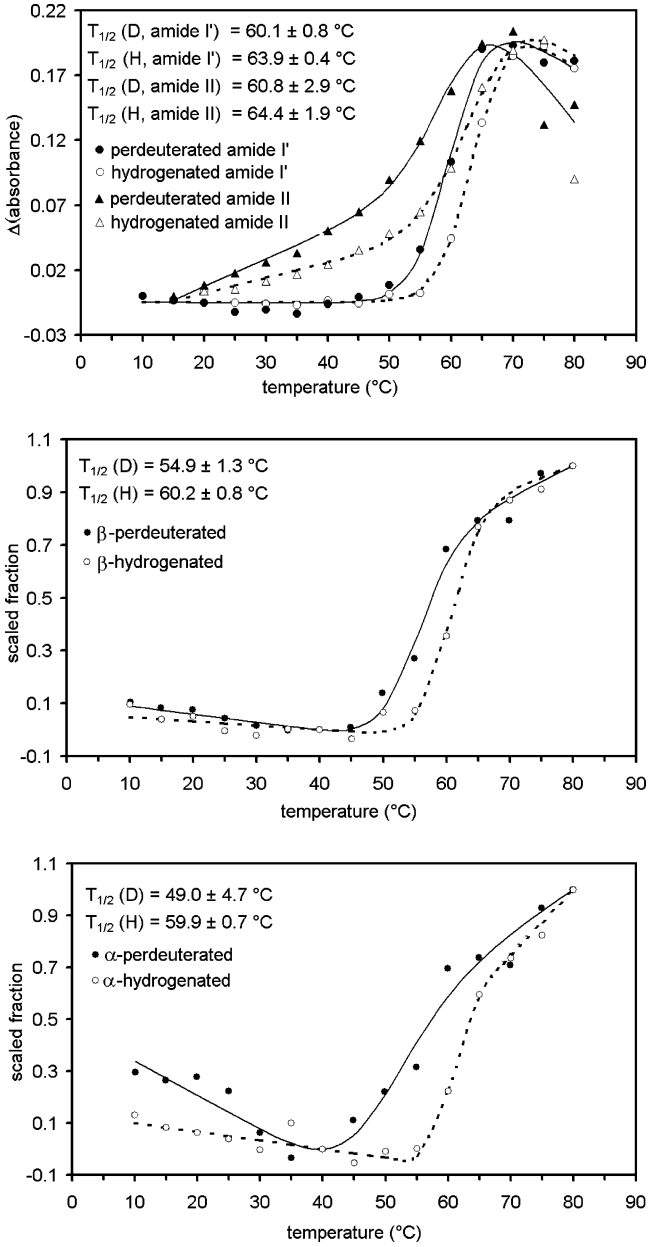

FIGURE 3: Thermal unfolding curves for hydrogenated (○, △) and perdeuterated (●, ▲) P450cam-(C334A) mutant corresponding (A, top) to the plot of the absorbance difference ΔA between the maximum and the minimum in the difference spectra, obtained from the area-normalized deconvoluted spectra (Figure 2) at temperature T minus the spectrum at 10 °C (ΔA(1616.04 cm^{-1} − 1657.50 cm^{-1}) for hydrogenated P450cam and ΔA(1609.29 cm^{-1} − 1640.63 cm^{-1}) for perdeuterated P450cam) (see the insets in Figure 2), versus the temperature (circles) and to the increasing amplitude of the negative band at about 1550 cm^{-1} (amide II) in the temperature difference spectra (not deconvoluted) with increasing temperature (triangles). (B, middle) and (C, bottom) correspond to the thermal unfolding curves determined from the plot of the increase of the β-sheet content and the decrease of the α-helix content versus the temperature. For a better comparison, all experimental curves are scaled to the same maximum value and fitted using eq 1 to estimate the $T_{1/2}$ value. The absolute values for an increase or a decrease of the content of secondary structure elements were taken from Tables 1 and 2.

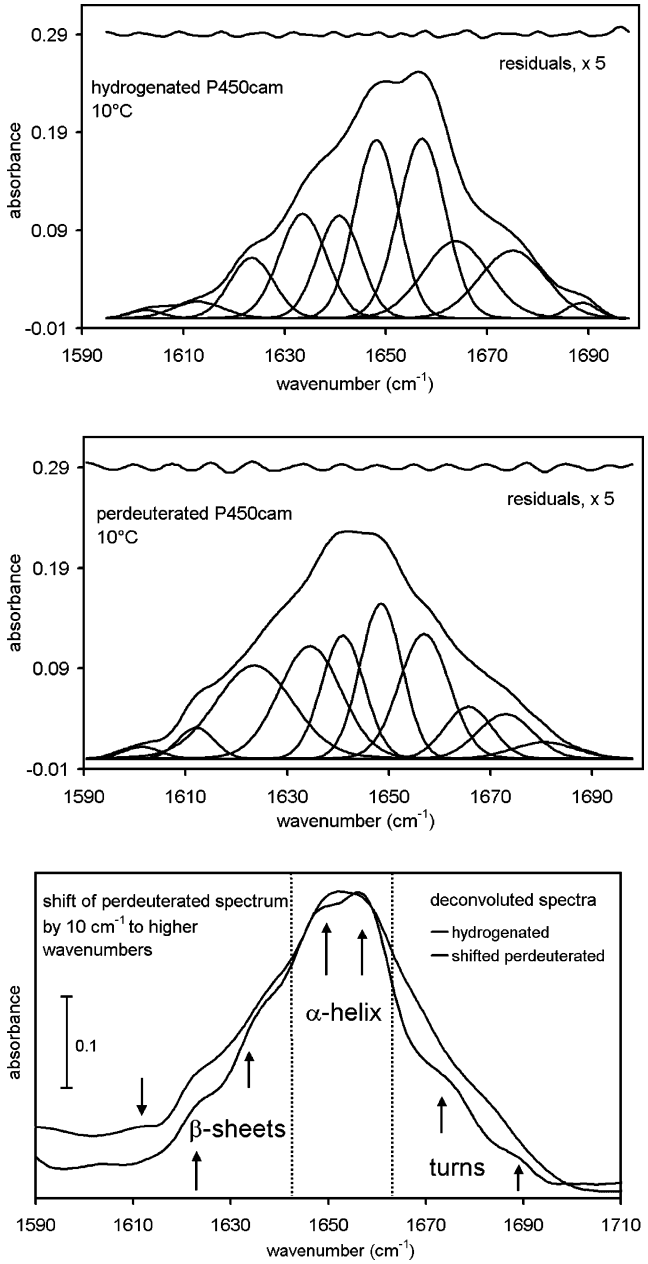

FIGURE 4: Deconvoluted amide I′ band at 10 °C and fit with Voigt functions for (A, top) hydrogenated and (B, middle) perdeuterated P450cam-(C334A) mutant. Numeric results of the fit are given in Tables 1 and 2. (C, bottom) Deconvoluted amide I′ spectrum of the perdeuterated protein (gray) shifted by 10 cm^{-1} to higher wavernumbers to demonstrate the feasibility of the assignments for secondary structure elements given in Tables 1 and 2.

protein which reveals a similar spectral pattern for the amide I′ bands (Figure 4C). Unfolding curves obtained from the plot of the fraction of β-sheet formation and the fraction of α-helix loss also confirm that the perdeuterated protein is less stable than the hydrogenated one. However, the absolute values for the unfolding half-transition temperatures for the β-sheets are about 4−5 °C lower (Figure 3B) compared to the $T_{1/2}$ obtained from the absorption amplitudes in the difference spectra (Figure 3A). The larger difference in $T_{1/2}$ by 10 °C for the α-helix content might result from the suboptimal fit of the unfolding curves (Figure 3C) because of the large relative contribution of the straight line in the low-temperature region in Figure 3C to the whole curve in the perdeuterated protein. This may also lead to the impression that the unfolding is less cooperative in the perdeuterated protein compared to the hydrogenated one. We hesitate to take this as significant because the enthalpy and entropy values obtained from the fit show a large error range (round values: ΔH(D) = 40 ± 20 kcal/mol and ΔS(D) = 130 ±

Table 1: Amide I′ Component Bands, Relative Integrated Intensities (Fraction), and Assignment to Secondary Structure Elements for Hydrogenated Cytochrome P450cam-(334A) Mutant (10 and 80 °C)[a]

10 °C		80 °C		
band position (cm^{-1})	fraction (%)	band position (cm^{-1})	fraction (%)	assignment
1602.6	1	1602.6	1	Arg side chain
1612.9 ± 6	2	1615.0 ± 0	3	Arg, Tyr side chain/β-sheets
1623.5 ± 1	7	1619.6 ± 6	18	β-sheets
1633.6 ± 3	13	1633.4 ± 2	16	β-sheets
1640.7 ± 1	11	1641.3 ± 3	10	unordered/3_{10}-helix
1648.1 ± 1	20	1648.5 ± 1	13	α-helix
1657.1 ± 1	21	1656.8 ± 1	15	α-helix
1663.8 ± 4	13	1664.9 ± 2	9	turns
1675.0 ± 4	11	1673.2 ± 4	10	turns
1688.7 ± 0	1	1683.1 ± 1	5	turns and high-wavenumber part of the β-sheets

[a] Error ranges are standard deviations obtained from the nonlinear least-squares fitting procedure.

Table 2: Amide I′ Component Bands, Relative Integrated Intensities (Fraction), and Assignment to Secondary Structure Elements for Perdeuterated Cytochrome P450cam-(334A) Mutant (10 and 80 °C)[a]

10 °C		80 °C		
band position (cm^{-1})	fraction (%)	band position (cm^{-1})	fraction (%)	assignment
1601.4 ± 1	1	1598.8 ± 0	1	Arg side chain
1612.1 ± 0	3	1610.6 ± 1	12	β-sheets
1623.5 ± 7	19	1622.5 ± 2	19	β-sheets
1634.5 ± 6	18	1633.9 ± 2	14	unordered /3_{10}-helix
1641.0 ± 1	13	1641.3 ± 1	11	α-helix
1648.4 ± 1	16	1648.5 ± 1	13	α-helix
1656.9 ± 2	16	1657.4 ± 2	15	turns
1665.6 ± 4	6	1666.3 ± 1	7	turns
1672.9 ± 6	6	1675.0 ± 1	7	turns
1680.5 ± 24	2	1682.5 ± 12	1	turns and high-wavenumber part of the β-sheets

[a] Error ranges are standard deviations obtained from the nonlinear least-squares fitting procedure.

80 cal/(K·mol) and $\Delta H(H) = 130 \pm 70$ kcal/mol and $\Delta S(H) = 400 \pm 200$ cal/(K·mol) for the perdeuterated and hydrogenated protein, respectively).

Unfolding curves obtained for the amide II band (Figure 3A) show a strong linear pretransition absorption change which would suggest that unfolding starts at much lower temperatures. However, the $T_{1/2}$ values obtained for the real transition are 64.4 and 60.8 °C for the hydrogenated and perdeuterated protein, respectively, and therefore match the values determined from the amide I′ band absorption difference amplitudes (Figure 3A).

CO Flash Photolysis. Replacing covalently bound hydrogen by deuterium in the protein has no effect on the band position or the band shape of the iron ligand CO stretching band at 1938.7 cm^{-1} in the absorption difference spectrum (Figure 5 and Table 3). Additionally, the integral extinction coefficient ϵ of the CO stretch band is identical in perdeuterated and hydrogenated P450cam-(C334), and in good agreement with the values determined from previous experiments (*19*). The inset in Figure 5 shows that the time trace for the CO ligand band rebinding is identical for the

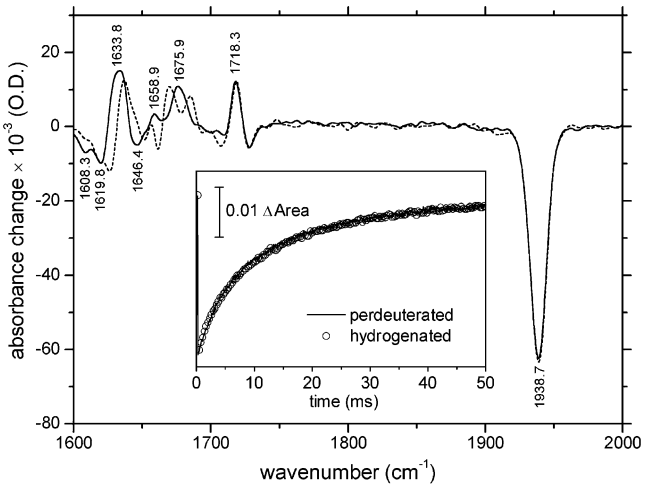

FIGURE 5: Infrared absorption difference spectra of the CO flash-photolyzed minus CO−iron-bound P450cam-(C334A) mutant protein: (solid line) perdeuterated protein, (dashed line) hydrogenated protein, both in 50 mM potassium phosphate buffer, pD 7.4, 50% (v/v) glycerol-d_3, 30 mM (1*R*)-camphor. Each spectrum is the average of the first 900 μs after laser photolysis. Peak positions are indicated for the perdeuterated protein. Inset: comparison of the scaled time traces for the time interval 0−20 ms for the CO ligand stretch band of hydrogenated (open circles) and perdeuterated (solid line) proteins.

perdeuterated and hydrogenated proteins. To determine the rebinding rate constant, the absorption difference changes as a function of time are described by the second-order rebinding model (eq 2), which fits very well the experimental data (Figure 6). Carbon monoxide-rebinding rate constants k_{on} are identical for the perdeuterated (8.9×10^4 M^{-1} s^{-1}) and the hydrogenated (8.3×10^4 M^{-1} s^{-1}) proteins when monitored at the CO stretch vibration band. The rate constants determined for the salt link, for turns and β-sheets, are identical with those of the CO ligand within experimental accuracy (Table 3). The rate constant determined for the α-helix in the perdeuterated protein is half the constant for the hydrogenated protein.

The position of the positive peak at ~1718 cm^{-1} does not change within the range of experimental accuracy due to perdeuteration, and the rate constant k_{on} (8.9×10^4 M^{-1} s^{-1}) matches that obtained for the rebinding process monitored at the CO ligand stretch mode band.

The turn-region signal for perdeuterated P450cam-(C334A) (1675.9 cm^{-1}) is at the same position as for the wild-type hydrogenated P450cam (1676.3 cm^{-1} (*19*)). However, hydrogenated P450cam-(C334A) shows two peaks in this region (1669.7 and 1685.0 cm^{-1}). It is not clear whether this split is real or just due to baseline noise.

Absorption changes in the α-helix region are only of small amplitude and are overlaid by noise. Therefore, signals at 1658.9 and 1646.4 cm^{-1} for perdeuterated P450cam-(C334A) and at 1661.6 and 1651.3 cm^{-1} for hydrogenated P450cam-(C334A) will not be interpreted.

The signal in the β-sheet region of perdeuterated P450cam-(C334A) is shifted by 5 cm^{-1} to lower wavenumbers (1633.8 cm^{-1}) compared to that of hydrogenated P450cam-(C334A) (1638.8 cm^{-1}). A negative peak at 1619.8 cm^{-1} for perdeuterated P450cam-(C334A) and at 1626.2 cm^{-1} for hydrogenated P450cam-(C334A) is shifted by approximately the same value (6.4 cm^{-1}).

Table 3: Band Positions and Rebinding Rate Constants at 300 K of Perdeuterated Cytochrome P450cam-(C334A)−Carbon Monoxide Complex from Time-Resolved Infrared Spectroscopy[a]

protein	[P450 −CO] (mM)	fraction photolyzed (%)	ϵ_{CO} (10^4 M^{-1} cm^{-2})	k_{on} (10^4 M^{-1} s^{-1}) CO ligand	salt link	turns	α-helix	β-sheet
perdeuterated P450cam-(C334A)	0.803	60.0	2.52 ± 0.01	8.9 ± 0.1 (1938.7 cm^{-1})	8.9 ± 0.3 (1718.3 cm^{-1})	8.0 ± 0.4 (1675.9 cm^{-1})	10.0 ± 3.5 (1658.9 cm^{-1})	8.4 ± 0.5 (1633.8 cm^{-1})
							12.5 ± 1.8 (1646.4 cm^{-1})	7.5 ± 0.6 (1619.8 cm^{-1})
								8.2 ± 0.6 (1608.3 cm^{-1})
hydrogenated P450cam-(C334A)	0.777	59.6	2.53 ± 0.01	8.3 ± 0.1 (1938.8 cm^{-1})	8.3 ± 0.2 (1718.7 cm^{-1})	9.4 ± 0.4 (1685.0 cm^{-1})	21.7 ± 2.9 (1661.6 cm^{-1})	8.2 ± 0.4 (1636.8 cm^{-1})
						7.5 ± 0.3 (1669.7 cm^{-1})	10.0 ± 1.7 (1651.3 cm^{-1})	8.9 ± 0.4 (1626.2 cm^{-1})

[a] Samples were in deuterated 50 mM potassium phosphate buffer, pD 7.4, 50% (v/v) glycerol-d_3, 1 mM (1*R*)-camphor. [CO] = 0.8 mM. Error ranges are standard deviations obtained from the nonlinear least-squares fitting procedure.

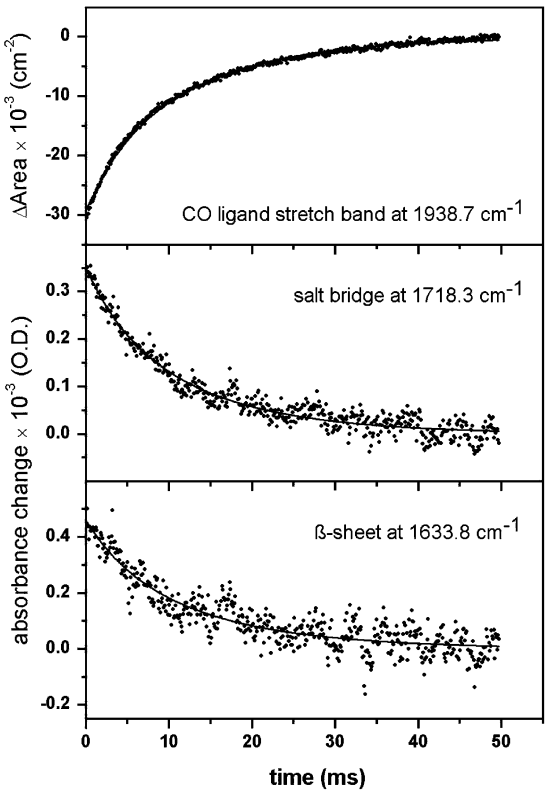

FIGURE 6: Carbon monoxide rebinding monitored by the absorbance change in the infrared spectrum of perdeuterated P450cam-(C334A) mutant bound with (1*R*)-camphor. Solid lines represent the fit with the second-order rebinding model (eq 2) of the experimental data. Upper panel: area of the CO stretch vibration band at 1938.7; cm^{-1}. Middle panel: peak amplitude at 1718.3 cm^{-1}. Lower panel: peak amplitude at 1633.8 cm^{-1}.

DISCUSSION

Perdeuteration of proteins is an increasingly used approach and requirement to characterize protein structures by NMR and neutron crystallography (*21*, *22*). In particular, for cytochrome P450s the advantage of neutron crystallography to detect water molecules and hydrogen bond networks would be of great importance to explore the P450 mechanism (*2*). However, many studies on P450cam (*23*, *24*) indicate that not only the specific spatial localization of water molecules but also the dynamics of water exchange between the heme pocket and the bulk solvent and the structural stability of the protein influence the catalytic efficiency of the enzyme. Comparative studies on hydrogenated and perdeuterated proteins will therefore be helpful to gain a deeper insight into structure−function relationships.

Effect of Perdeuteration on Infrared Spectra of P450cam. The shift of the amide I′ band to lower wavenumbers by ∼10 cm^{-1} due to perdeuteration of the amino acid side chains can easily be explained by the increased mass. The amide I band results mainly from the stretch mode of the peptide C═O group (*16*). In the simplified harmonic oscillator model for the C═O vibration with the force constant *k*, the replacement of covalently bound hydrogens by deuterium leads to a higher effective mass $m_{C'}$ for the carbon atom, resulting in a higher reduced mass μ whose square root is inversely related to the vibration frequency (*25*):

$$\nu = (1/2\pi)(k/\mu)^{1/2}, \qquad \mu = \frac{(m_{C'}m_O)}{(m_{C'} + m_O)} \tag{3}$$

For the amide II band, which is the N−H(D) bending admixed by C−N stretching modes (*16*), the mass effect is more complex, resulting effectively in a shift to higher wavenumbers. At first glance one would expect that an amide II band corresponding to N−H bending should not exist at all because the proteins were dialyzed against D_2O buffer. However, because of structural rigidity of proteins, exchangeable hydrogens in the protein core are not completely replaced by deuterons during dialysis, even not when multiple D_2O/H_2O exchanges were performed over many hours as done in this study. This is also true for the perdeuterated protein, which was even expressed in a D_2O medium. Similar to the hydrogenated protein, the perdeuterated protein was purified in H_2O buffers over several days, and therefore, the exchangeable deuterons (i.e., N−D) were more or less replaced by hydrogens which were not completely back-exchanged during the dialysis against the D_2O buffer for preparation of the IR samples. However, because there are still deuterons in the protein core, one expects that the maximal temperature-induced change of the amide II amplitude in the perdeuterated protein should be smaller than in the hydrogenated protein. Indeed, the ratio of the amplitude of the amide II change at ∼1550 cm^{-1} to the amplitude change of the β-sheets at ∼1610 cm^{-1} (D), respectively ∼1620 cm^{-1} (H), is only ∼0.23 for the perdeuterated protein but ∼0.83 for the hydrogenated protein.

Perdeuteration of tyrosine leads to a strong downshift of the ring vibration by ∼90 cm^{-1} from ∼1518 cm^{-1} to a split band at 1442 and 1416 cm^{-1} (in H_2O buffer) (*26*). Such a

large shift is also expected for D_2O buffer used in our experiments and explains why the signal at 1515 cm^{-1} is lost in the perdeuterated protein. The signal for the perdeuterated tyrosine cannot be seen because of the overlap with the strong amide II′ band at about 1450 cm^{-1}.

Effect of Perdeuteration on the Secondary Structure Composition of P450cam. The secondary structure composition of the hydrogenated P450cam-(C334A) mutant at 10 °C, estimated from the relative area of the single amide I′ bands (Table 1), is similar to that of the wild-type protein (values in parentheses (*17*)): 22% (21%) for β-sheets, 41% (40%) for α-helix, 11% (14%) for unordered structure/3_{10}-helix, 24% (19%) for turns, and 1% (2%) for overlay of turns and the high-frequency part of the β-sheet absorption. Perdeuteration of the mutant protein leads to 22% for β-sheets, 29% for α-helix, 18% for unordered structure/3_{10}-helix, 28% for turns, and 2% for overlay of turns and the high-frequency part of the β-sheet absorption (Table 2). It seems that about 12% of the α-helix content of the hydrogenated protein is lost in favor of an increase in unordered structure/3_{10}-helix and turn structures. Whether this loss of 12% in α-helix content must be regarded as significant is difficult to decide on the basis of only the IR data because the width of the fitted band assigned to unordered structure/3_{10}-helix is broader in the perdeuterated protein ($\nu = 1634.5$ cm^{-1}, $\Delta\nu_{1/2} = 15$ cm^{-1}) and overlaps more with the α-helix band than in the hydrogenated protein ($\nu = 1640.8$ cm^{-1}, $\Delta\nu_{1/2} = 10$ cm^{-1}) (compare parts A and B of Figure 4). Therefore, it may contain few contributions which should belong to α-helix content. However, assuming that in solution one amino acid at both ends of each of the 14 helices in P450cam (*2*) would be unwound in the perdeuterated protein, one would expect a decrease of the α-helix content by 6−7% and a corresponding increase in turn structures. Under this condition the overall tertiary structure may not change. Our preliminarily resolved crystal X-ray analysis shows a similar structure for both proteins (unpublished results).

Effect of Perdeuteration on Thermal Unfolding of P450cam. All unfolding curves, independently of whether they are obtained from the amide I or amide II bands, show that the perdeuterated protein is less stable than the hydrogenated one, which means $T_{1/2}$ (perdeuterated) < $T_{1/2}$ (hydrogenated). This finding is in agreement with observations on other proteins (*11*, *27*, *28*). In particular, one finds for proteins in H_2O buffer that the difference between $T_{1/2}$ of the perdeuterated proteins and $T_{1/2}$ of the hydrogenated proteins ($|\Delta T_{1/2}|$) is larger the lower the absolute value of $T_{1/2}$ of the hydrogenated proteins appears to be (*11*) (Figure 7). Our data for P450cam-(C334A) fit in this relation (inset of Figure 7). However, P450cam was studied in D_2O buffer. Plots of the only two available values of $\Delta T_{1/2}$ for other proteins studied in D_2O are off-line, which might suggest that, if our data for P450cam are considered, for D_2O buffer the inverse effect may be valid. There are however too few data to draw a definite conclusion.

Nevertheless, perdeuterated proteins are generally less stable against thermal unfolding, which looks curious at first glance, because it is well-known that proteins in D_2O buffer show a higher thermal stability (*27*, *29*−*31*) than in H_2O buffer, and that is also the case for P450cam (*17*). The explanation of this apparent contradiction is straightforward.

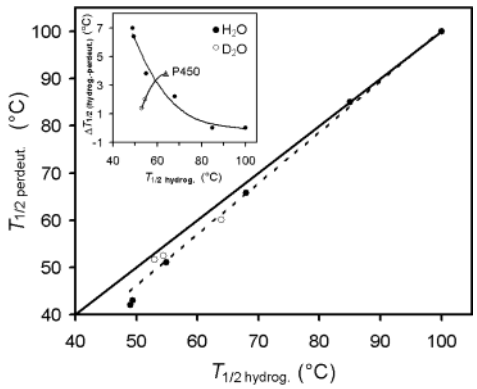

FIGURE 7: Midpoint transition temperature $T_{1/2,perdeut}$ of thermal unfolding of perdeuterated proteins versus the midpoint transition temperature $T_{1/2,hydrog}$ of the hydrogenated proteins in H_2O or D_2O buffer. The values of the following proteins are included: protiophycocyanine from *Phormidium luridum* (49.4 °C in H_2O; 54.5 °C in D_2O), deuteriophycocyanine from *P. luridum* (43 °C in H_2O; 52.5 °C in D_2O), protiophycocyanine from *Plectonema calothricoides* (49 °C in H_2O; 53 °C in D_2O), deuteriophycocyanine from *P. calothricoides* (42 °C in H_2O; 51.6 °C in D_2O) (*27*), protioglutathione S-transferase (54.9 °C in H_2O), deuterioglutathione S-transferase (51 °C in H_2O) (*11*), alkaline phosphatase from *E. coli* (85 °C for hydrogenated and perdeuterated protein in H_2O); ribonuclease from *Fremyella diplosiphon* (100 °C for hydrogenated and perdeuterated protein in H_2O) (*28*), hydrogenated cytochrome P450cam-(C334A) (63.9 °C in D_2O), perdeuterated cytochrome P450cam-(C334A) (60.1 °C in D_2O) (gray filled triangle, this paper). The solid black line corresponds to the hypothetical 45° line if $T_{1/2}$ is identical for the perdeuterated and hydrogenated proteins. Inset: difference in $T_{1/2}$ of hydrogenated minus perdeuterated proteins for H_2O and D_2O buffer versus the absolute value of $T_{1/2}$ for the hydrogenated proteins.

Substitution of H_2O by D_2O affects only the exchangeable hydrogens which form the hydrogen bonds in proteins. Hydrogen bonds are strengthened by deuteration because the larger mass of D leads to a lower vibration frequency, respectively lower bond energy for the donator−D bond (peptide N−D) compared to the donator−H bond (peptide N−H). This facilitates the bonding to the acceptor atom (peptide C═O). In contrast, the exchange of the covalently bound hydrogens by deuterium reduces essentially the hydrophobic interactions between the amino acids. It has been argued that the lower zero-point energy of the −C−D bond compared to −C−H is accompanied by a reduction of the bond vibration amplitude. This diminishes the steric constraints for forming the activated complex and therefore diminishes the activation energy for thermal unfolding of the protein (*11*, *27*). One may consider that a weakening of a −C−H covalent bond by substitution of H by D could facilitate the interaction with the lone pairs of water molecules in a "hydrogen-bond-like", mode but the polarization of the covalent −C−H bond is too weak to make a significant contribution.

In agreement with studies on many other proteins (*29*, *32*), and also on the wild-type P450cam (*17*, *33*), thermal unfolding of P450cam-(C334A) leads to a loss of α-helix content of 13% (5%) and an increase of β-sheet content of about 15% (9%) for the hydrogenated (perdeuterated) protein. The mismatch of the extent of α-helix content loss (5%) with the β-sheet content increase (9%) for the perdeuterated protein may result in part from the too strong overlap of the fitted band assigned to unordered structure/3_{10}-helix with the one of the two bands assigned to the α-helix as discussed

above. The content of unordered structure/3_{10}-helix decreases by 4% during unfolding (1% in the hydrogenated protein) (compare Tables 1 and 2). Part of this loss may actually belong to the loss of α-helix. The β-sheet content at high temperatures is mainly caused by intermolecular β-sheets of the aggregated protein detected at the characteristic infrared bands at ~1620 and ~1684 cm^{-1} (*16*, *29*). Thermal unfolding of P450 proteins is irreversible (*34*). For the wild-type P450cam we had already detected by scanning calorimetric studies that unfolding proceeds via three unfolding units with transition temperatures at 48.5, 57.3, and 61.7 °C in H_2O buffer (*35*, *36*). In D_2O buffer all or some of these midpoint transition temperatures might be shifted to higher values. The present study reveals a value of ~64 °C for the main transition in the hydrogenated protein and ~60 °C for the perdeuterated protein. However, the unfolding curves obtained from the amide II band, which is generally more sensitive to the initial steps of unfolding, indicate that already at lower temperatures pretransitions occur which may reflect the multiunit unfolding behavior. Indeed, the temperature-induced difference spectra in the insets of Figure 2 show between 10 and 50 °C a pattern qualitatively different from that for temperatures higher than 50 °C, which must result from another type of structural change. One type of structural change is certainly the low-spin state to high-spin state transition (*23*, *24*) appearing between 10 and 40 °C. This behavior is the same in the hydrogenated and the perdeuterated proteins.

Effect of Perdeuteration on CO-Ligand-Binding Kinetics. We have previously reported (*19*) that CO flash photolysis studies combined with step-scan time-resolved FTIR spectroscopy provide two kinds of important information. First, one obtains complete spectra at each time point, allowing the structural changes involved in CO binding to be assigned, and second, one can determine the time traces at each infrared signal. The shift of all signals with wavenumbers lower than 1700 cm^{-1} due to perdeuteration of P450cam clearly demonstrates that these signals arise from the protein whose structure is changed upon CO binding. In contrast, the signal at ~1718 cm^{-1} is unchanged. We have previously suggested that this signal reflects the C═O stretch vibration of the carboxyl acid group of the 7-propionic acid side chain of the heme, which is involved in a salt bridge with Arg299 and Asp297 (*19*). The heme in the perdeuterated protein is not deuterated because hydrogenated δ-aminolevulinic acid as heme precursor was used. Thus, the same position of this band for the hydrogenated and perdeuterated protein clearly confirms that this signal originates from the heme carboxyl group and not from an aspartatic or glutamic acid in the protein. The stretch vibration wavenumber of the iron CO ligand is also identical in the hydrogenated and perdeuterated protein, which indicates that the CO ligand has no van der Waals contact to any amino acid side chain as is also confirmed by the crystal structure of the wild-type P450cam−CO complex (*37*).

In light of the lower thermal stability of the perdeuterated protein compared to the hydrogenated one as discussed above, the most interesting finding is that the hydrogenated and the perdeuterated proteins show the same kinetics and rate constant k_{on} for the rebinding of the dissociated CO ligand [(perdeuterated) 8.9×10^4 M^{-1} s^{-1} and (hydrogenated) 8.3×10^4 M^{-1} s^{-1} when monitored at the CO ligand stretch vibration band (Figure 6)). The respective rate constants for the CO ligand, the salt bridge, turns, and β-sheet signals are equal within experimental accuracy (Table 3), indicating that local CO-ligand-binding and global protein dynamics are the same. The somewhat larger value for one of the α-helix signals in the hydrogenated protein [$(21.7 \pm 2.9) \times 10^4$ M^{-1} s^{-1} (1661.6 cm^{-1})] should not be considered as significant because of the very small amplitude of the signal and therefore the bad signal-to-noise ratio as mentioned in the Results.

At temperatures higher than the glass transition temperature (~200−220 K) the photodissociated CO ligand leaves the heme pocket and rebinds from the bulk solvent reflected in the dependence of the rate on the CO concentration (*38*) analogous to the situation in stopped-flow experiments (*39*). Results of stopped-flow experiments for the CO binding in wild-type P450cam as a function of the hydrostatic pressure suggested that CO binding in the camphor-bound protein is statistically disfavored and therefore slow when compared to that in the substrate-free protein. The search for the optimal place near the heme (so-called B state (*40*)) before the CO−iron bond is formed appears to be rate-limiting (*39*). The same rate constants for the CO binding in the hydrogenated and perdeuterated camphor-bound proteins therefore suggest that hydrophobic interactions between the amino acid residues which are affected by perdeuteration (*11*, *27*) do not play a major role in finding this place near the heme.

CONCLUSIONS

The present results of the comparative FTIR studies of hydrogenated and perdeuterated P450cam-(C334A) show that the structure and dynamics of the proteins at ambient conditions for temperature and pressure are very similar. Structural information obtained from neutron crystallography on perdeuterated P450cam will therefore be representative also for the proteins under normal hydrogenated conditions and can be used for analyses of structure−function relationships. However, when thermal unfolding properties are investigated, one has to consider that perdeuteration lowers the transition temperature.

ACKNOWLEDGMENT

Stephen G. Sligar, University of Illinois, Urbana, is acknowledged for providing the pUS200 vector for the wild-type P450cam to F.M. We thank the ILL/EMBL staff of the Deuteration Laboratory (Grenoble) for assistance and Thomas Franz and Xinping Li for the mass spectrometry analysis (EMBL−Heidelberg). We thank O. Ristau (MDC, Berlin) for assistance in fitting the thermal unfolding curves. We are grateful to Ilme Schlichting (Max-Planck-Institute for Medical Research, Heidelberg) for helpful discussions and exchange of ideas about neutron crystallography on P450cam.

REFERENCES

1. Ortiz de Montellano, P. R. (1995) *Cytochrome P450: Structure, Mechanism and Biochemistry*, 2nd ed., Plenum, New York.
2. Schlichting, I., Berendzen, J., Chu, K., Stock, A. M., Maves, S. A., Benson, D. E., Sweet, R. M., Ringe, D., Petsko, G. A., and Sligar S. G. (2000) The catalytic pathway of cytochrome P450cam at atomic resolution, *Science 286*, 1615−1622.
3. Niimura, N., Minezaki, Y., Nonaka, T., Castagna, J. C., Cipriani, F., Hoghoj, P., Lehmann, M. S., and Wilkinson, C. (1997) Neutron

Laue diffractometry with an imaging plate provides an effective data collection regime for neutron protein crystallography, *Nat. Struct. Biol. 4*, 909−914.
4. Bon, C., Lehmann, M. S., and Wilkinson, C. (1999) Quasi-Laue neutron-diffraction study of the water arrangement in crystals of triclinic hen egg-white lysozyme, *Acta Crystallogr. D55*, 978−87.
5. Habash, J., Raftery, J., Nuttall, R., Price, H. J., Wilkinson, C., Kalb, A. J., and Helliwell, J. R. (2000) Direct determination of the positions of the deuterium atoms of the bound water in concanavalin A by neutron Laue crystallography, *Acta Crystallogr. D56*, 541−550.
6. Shu, F., Ramakrishnan, V., and Schoenborn, B. P. (2000) Enhanced visibility of hydrogen atoms by neutron crystallography on fully deuterated myoglobin, *Proc. Natl. Acad. Sci. U.S.A. 97*, 3872−3877.
7. Coates, L., Erskine, P. T., Wood, S. P., Myles, D. A., and Cooper, J. B. (2001) A neutron Laue diffraction study of endothiapepsin: implications for the aspartic proteinase mechanism, *Biochemistry 40*, 13149−13157.
8. Ostermann, A., Tanaka, I., Engler, N., Niimura, N., and Parak, F. G. (2002) Hydrogen and deuterium in myoglobin as seen by a neutron structure determination at 1.5 Å resolution, *Biophys. Chem. 95*, 183−193.
9. Chatake, T., Ostermann, A., Kurihara, K., Parak, F. G., and Niimura, N. (2003) Hydration in proteins observed by high-resolution neutron crystallography, *Proteins 50*, 516−523.
10. Engler, N., Ostermann, A., Niimura, N., and Parak, F. G. (2003) Hydrogen atoms in proteins: positions and dynamics, *Proc. Natl. Acad. Sci. U.S.A. 100*, 10243−10248.
11. Brockwell, D., Yu, L., Cooper, S., McCleland, S., Cooper, A., Attwood, D., Gaskell, S. J., and Barber, J. (2001) Physicochemical consequences of the perdeuteriation of glutathione S-transferase from *S. japonicum*, *Protein Sci. 10*, 572−580.
12. Unger, B. P., Gunsalus, I. C., and Sligar, S. G. (1986) Nucleotide sequence of the *Pseudomonas putida* cytochrome P-450cam gene and its expression in *Escherichia coli*, *J. Biol. Chem. 261*, 1158−1163.
13. Lipscomb, J. D., Harrison, J. E., Dus, K. M., and Gunsalus, I. C. (1978) Cytochrome P450cam: SS dimer and SH derivative reactivities, *Biochem. Biophys. Res. Commun. 83*, 771−778.
14. Nickerson, D. P., and Wong, L.-L. (1997) The dimerization of *Pseudomonas putida* cytochrome P450cam: practical consequences and engineering of a monomeric enzyme, *Protein Eng. 10*, 1357−1361.
15. Lumry, R., Smith, E. L., and Glantz, R. R. (1951) Kinetics of carboxypeptidase action. Effect of various extrinsic factors on kinetic parameters, *J. Am. Chem. Soc. 73*, 4330−4340.
16. Jung, C. (2000) Insight into protein structure and protein−ligand recognition by Fourier transform infrared spectroscopy, *J. Mol. Recognit. 13*, 325−351.
17. Mouro, C., Jung, C., Bondon, A., and Simonneaux, G. (1997) Comparative Fourier transform infrared studies of the secondary structure and the CO heme ligand environment in cytochrome P-450cam and cytochrome P-420cam, *Biochemistry 36*, 8125−8134.
18. Schulze, H., Hui Bon Hoa, G., Helms, V., Wade, R. C., and Jung, C. (1996) Structural changes in cytochrome P-450cam effected by the binding of the enantiomers (1R)-camphor and (1S)-camphor, *Biochemistry 35*, 14127−14138.
19. Contzen, J., and Jung, C. (1998) Step-scan time-resolved FTIR spectroscopy of cytochrome P-450cam carbon monoxide complex: a salt link involved in the ligand-rebinding process, *Biochemistry 37*, 4317−4324.
20. Contzen, J., and Jung, C. (1999) Changes in secondary structure and salt links of cytochrome P-450cam induced by photoreduction: a Fourier transform infrared spectroscopic study, *Biochemistry 38*, 16253−16260.
21. Gutberlet, Th., Heinemann, U., and Steiner, M. (2001) Protein crystallography with neutrons−status and perspectives, *Acta Crystallogr. D57*, 349−354.
22. Savenkova, M. I., Satterlee, J. D., Erman, J. E., Siems, W. F., and Helms, G. L. (2001) Expression, purification, characterization, and NMR studies of highly deuterated recombinant cytochrome c peroxidase, *Biochemistry 40*, 12123−12131.
23. Schulze, H., Hui Bon Hoa, G., and Jung, C. (1997) Mobility of norbornane-type substrates and water accessibility in cytochrome P-450cam, *Biochim. Biophys. Acta 1338*, 77−92.
24. Jung, C., Kozin, S. A., Canny, B., Chervin, J.-C., and Hui Bon Hoa, G. (2003) Compressibility and uncoupling of cytochrome P450cam: high-pressure FTIR and activity studies, *Biochem. Biophys. Res. Commun. 312*, 197−203.
25. Atkins, P. W. (1986) *Physical Chemistry*, 3rd ed., Oxford University Press, Oxford, U.K.
26. Hellwig, P., Pfitzner, U., Behr, J., Rost, B., Pesavento, R. P., Donk, W. V., Gennis, R. B., Michel, H., Ludwig, B., and Mäntele, W. (2002) Vibrational modes of tyrosines in cytochrome c oxidase from *Paracoccus denitrificans*: FTIR and electrochemical studies on Tyr-D_4-labeled and on Tyr280His and Tyr35Phe mutant enzymes, *Biochemistry 41*, 9116−9125.
27. Hattori, A., Crespi, H. L., and Katz, J. J. (1965) Effect of side-chain deuteration on protein stability, *Biochemistry 4*, 1213−1225.
28. Rokop, S., Gajda, L., Parmerter, S., Crespi, H. L., and Katz, J. J. (1969) Purification and characterization of fully deuterated enzymes, *Biochim. Biophys. Acta 191*, 707−715.
29. Dong, A., Kendrick, B., Kreilgard, L., Matsuura, J., Manning, M. C., and Carpenter, J. F. (1997) Spectroscopic study of secondary structure and thermal denaturation of recombinant human factor XIII in aqueous solution, *Arch. Biochem. Biophys. 347*, 213−220.
30. Kuhlman, B., and Raleigh, D. P. (1998) Global analysis of the thermal and chemical denaturation of the N-terminal domain of the ribosomal protein L9 in H_2O and D_2O. Determination of the thermodynamic parameters, $\Delta H°$, $\Delta S°$, and $\Delta Cp°$ and evaluation of solvent isotope effects, *Protein Sci. 7*, 2405−2412.
31. Harrington, W. F., and Von Hippel, P. H. (1961) Formation and stabilization of the collagen-fold, *Arch. Biochem. Biophys. 92*, 100−112.
32. Goossens, K., Haelewyn, J., Meersman, F., De Ley, M., and Heremans, K. (2003) Pressure- and temperature-induced unfolding and aggregation of recombinant human interferon-gamma: a Fourier transform infrared spectroscopy study, *Biochem. J. 370*, 529−535.
33. Nölting, B. O., Jung, C., and Snatzke, G. (1992) Multichannel circular dichroism investigations of the structural stability of bacterial cytochrome P-450, *Biochim. Biophys. Acta 1100*, 171−176.
34. Jung, C., Bendzko, P., Ristau, O., and Gunsalus, I. C. (1985) Thermodynamic studies on different cytochrome P-450 proteins, in *Cytochrome P450-Biochemistry and Induction* (Vereczky, L., and Magyar, K., Eds.) pp 19−22, Akademia Kiado, Budapest.
35. Pfeil, W., Nölting, B. O., and Jung, C. (1993) Apocytochrome P450cam is a native protein with some intermediate-like properties, *Biochemistry 32*, 8856−8862.
36. Jung, C., Pfeil, W., Köpke, K., Schulze, H., and Ristau, O. (1994) Conformational states and substates of cytochrome P450cam−Insight in protein dynamics and folding, in *Cytochrome P450: Biochemistry, Biophysics and Molecular Biology* (Lechner, M. C., Ed.), pp 543−546, John Libbey Eurotext, Paris.
37. Raag, R., and Poulos, T. L. (1989) Crystal structure of the carbon monoxide-substrate-cytochrome P-450CAM ternary complex, *Biochemistry 28*, 7586−7592.
38. Contzen, J., Ristau, O., and Jung, C. (1996) Time-resolved Fourier-transform infrared studies of the cytochrome P-450cam carbon-monoxide complex bound with (1R)-camphor and (1S)-camphor substrate, *FEBS Lett. 383*, 13−17.
39. Jung, C., Bec, N., and Lange, R. (2002) Substrates modulate the rate-determining step for CO binding in cytochrome P450cam (CYP101): A high-pressure stopped-flow study, *Eur. J. Biochem. 269*, 2989−2996.
40. Jung, C. (2002) Cytochrome P-450-CO and substrates: lessons from ligand binding under high pressure, *Biochim. Biophys. Acta 1595*, 309−328.

BI049418Q